



# Settling versus mixing in stratified shear flows

Nicolaos Petropoulos<sup>1,†</sup>, Colm-cille P. Caulfield<sup>1,2</sup>, Patrice Meunier<sup>3</sup> and Emmanuel Villiermaux<sup>3,4</sup>

<sup>1</sup>Department of Applied Mathematics and Theoretical Physics, University of Cambridge, Cambridge CB3 0WA, UK

<sup>2</sup>Institute for Energy and Environmental Flows, University of Cambridge, Cambridge CB3 0EZ, UK

<sup>3</sup>Aix Marseille Université, CNRS, Centrale Marseille, IRPHE UMR 7342, 13384 Marseille, France

<sup>4</sup>Institut Universitaire de France, 75005 Paris, France

(Received 9 June 2023; revised 11 September 2023; accepted 21 September 2023)

We study the coupled settling, deformation and mixing dynamics of a dense blob of fluid falling in an axially (vertically) linearly stratified Taylor–Couette cell (operated in a laminar stable regime). This configuration allows the independent analysis of stretching dynamics, driven by radial (horizontal) velocity variations, and settling dynamics, driven by buoyancy forces associated with vertical density variations. As the blob settles, it is stretched in the horizontal plane and forms an elongated lamella. Through the competing effects of transverse compression of the lamella due to this shear-induced stretching and broadening due to diffusion, the lamella irreversibly mixes with ambient fluid, thus progressively adjusting its own density towards that of the ambient fluid. Eventually, the lamella settling stops at a final equilibrium position that depends on the ambient vertical density gradient and the rate at which it has been deformed by the horizontal shear. We show how this final position is determined by stretching-enhanced diffusion, i.e. mixing. We demonstrate that a theoretical mixing model compares favourably with experiments with various Froude numbers (quantifying the relative strength of the horizontal shear and the vertical stratification) and construct a new criterion for the energetic ‘efficiency’ of this mixing process that explicitly captures its inherently diffusive character.

**Key words:** laminar mixing

## 1. Introduction

Mixing, i.e. the way in which a composition or scalar field irreversibly evolves from a segregated state towards homogeneity, is a key process for a large variety of settings with

† Email address for correspondence: [np546@cam.ac.uk](mailto:np546@cam.ac.uk)

length and time scales spanning orders of magnitude. A particularly significant setting is within geophysical flows, as both the atmosphere and the oceans are (on average) vertically stratified in density. As the average density gradient is anti-parallel to the (vertical) direction in which gravity acts, fluid elements vertically displaced from their equilibrium position experience a restoring buoyancy force which tends to bring them back to their equilibrium. However, buoyancy forces can also trigger a wide range of instabilities, inducing relatively large-scale and nominally reversible ‘stirring’ motions that actually increase the rate of (irreversible) mixing and thus affect (and typically reduce) the driving buoyancy forces of the stirring. When classified in this way, mixing in stratified flows is an interesting example of a ‘two-way coupling’ phenomenon. Stirring enhances mixing but is itself sensitive to the effects of mixing, as the scalar being mixed is ‘dynamic’, in the sense that its instantaneous spatial distribution affects the fluid flow (Caulfield 2021).

Understanding (and quantifying) irreversible stratified mixing is exceptionally important because of its considerable (and still somewhat uncertain) impact on basin-scale transport of heat and salinity in the oceans (Munk 1966; Wunsch & Ferrari 2004), a key component of the global climate system. There has been a huge amount of effort devoted to constructing useful and robust parametrisations of this mixing (Gregg *et al.* 2018; Caulfield 2021). In particular, mixing properties, especially a measure of mixing efficiency, are often described from an energetic viewpoint, as irreversible mixing of a statically stable density distribution tends to increase the ‘background potential energy’ (i.e. the minimum potential energy associated with the notional adiabatic rearrangement of density parcels (Winters *et al.* 1995)).

Therefore, measures of the efficiency of mixing are often quantified cumulatively as the proportion of injected kinetic energy that irreversibly increases the background potential energy, or instantaneously in terms of the relative size of the rate of destruction of ‘available’ potential energy (i.e. the difference between the actual potential energy and the background potential energy, notionally available to drive motion) to the dissipation rate of kinetic energy. Although this energetic approach to mixing quantification is appealing and can (in some circumstances) be connected directly to actual irreversible scalar mixing via the diffusive reduction in scalar variance (Caulfield 2021), there are non-trivial issues with this conflation of energy reservoir exchanges with diffusive mixing, which is not generically appropriate (Tailleux 2013). Even in the simplest case of a ‘Boussinesq’ fluid with kinematic viscosity  $\nu$  and a linear single-component equation of state (i.e. where the density is linearly related to a single scalar with diffusivity  $D$ ), this energetic approach to describing mixing has no obvious way to describe or quantify the widely observed dependence of mixing properties on the fluid’s Prandtl number  $Pr = \nu/D$  (Smyth, Moum & Caldwell 2001; Salehipour, Peltier & Mashayek 2015; Riley, Couchman & de Bruyn Kops 2023) and hence on the molecular properties of the scalar being mixed. Such a result suggests that the exceptionally small-scale diffusive processes are (perhaps unsurprisingly) crucially important for mixing even in (strongly) turbulent flows.

There is thus room for studying stratified mixing where the dynamic effects of buoyancy forces on the fluid flow are decoupled in a controlled way. We focus on a particular ‘one-way coupling’ situation where the large-scale flow is externally imposed and is unaffected by buoyancy forces. We consider the settling of an initially spherical and relatively dense blob of fluid in a vertically (axially) stratified Taylor–Couette cell, with a constant linear density gradient and hence constant buoyancy frequency  $N$  given by  $N^2 = (-g/\rho_0) d\bar{\rho}/dz$ , where  $g$  is the gravitational acceleration,  $\bar{\rho}$  is the horizontally averaged density and  $\rho_0$  is some reference density. This configuration allows the independent analysis of stretching dynamics (driven by radial (horizontal) velocity

variations) and settling dynamics (driven by buoyancy forces associated with vertical density variations), which, crucially, do not affect the macroscopic flow velocity distribution. As the blob settles, it is stretched in the horizontal plane and forms an elongated lamella. Through the competing effects of compression transverse to the lamella due to this shear-induced stretching and broadening due to diffusion, the lamella irreversibly mixes with ambient fluid, thus progressively adjusting its own density towards that of the ambient fluid. The settling stops at a final equilibrium position, where the blob has the same density as the ambient fluid and so there is zero buoyancy force, that depends on the ambient vertical density gradient and the deformation rate (by the horizontal shear) of the blob.

This process can thus be thought of as an idealisation of the final relatively small-scale irreversible mixing that occurs following some dynamically significant stirring associated with a larger-scale flow, and thus has the opportunity to capture the key interplay between stretching and diffusion at the heart of a small-scale description of mixing. Indeed, this process can be studied quantitatively thanks to the lamellar representation of mixing. Decomposing a scalar field into an ensemble of lamellae that concomitantly stretch, diffuse and aggregate has allowed significant progress (Villermaux 2019). At the scale of a unique lamella, two phenomena compete: kinematic deformation (at some shear rate  $\gamma$  given by the macroscopic flow), and diffusive broadening (at some rate  $D/s_0^2$ , where  $s_0$  is an initial characteristic blob length scale and  $D$  is the diffusion coefficient of the scalar field). The ratio of these two rates defines an appropriate Péclet number,

$$Pe := \frac{\gamma s_0^2}{D} = RePr, \tag{1.1}$$

where  $Re := \gamma s_0^2/\nu$  ( $\nu$  being the kinematic viscosity of the fluid) is the appropriate Reynolds number for the blob's evolution and  $Pr := \nu/D$  is the molecular Prandtl number. When  $Pe \gg 1$ , the mixing time  $t_S \sim \gamma^{-1}\mathcal{F}(Pe)$  is of order  $\gamma^{-1}$ , and importantly it is significantly smaller than the diffusion time  $s_0^2/D$  and depends on the diffusion properties of the scalar being mixed through a weak function  $\mathcal{F}(Pe)$  of the Péclet number (Villermaux 2019). In a simple shear,  $t_S \sim \gamma^{-1}Pe^{1/3}$ , and the post-mixing time concentration and width of the lamella are well understood and documented (Ranz 1979; Meunier & Villermaux 2003; Souzy *et al.* 2018).

Simplistically, it seems reasonable that the (appropriately non-dimensionalised) final equilibrium position of such a blob would involve some combination of  $1/N$  (the buoyancy time scale) and  $t_S$  (the density homogenisation time scale, independent of  $N$ ). However, particularly when  $Pr \gg 1$  (and so  $Re \ll 1$  while  $Pe \gg 1$ ), viscous drag sets the settling velocity, and so it is at least plausible that the equilibrium position depends on  $Re$  too. To investigate the dependence on the various flow parameters of the final equilibrium position, and hence the flow's mixing properties, the rest of this paper is organised as follows. The experimental set-up and measurements are reported in § 2. A theoretical model for the concomitant settling and deforming lamella in a viscous stratified shear flow is introduced in § 3 and compared with the experiments. Some implications of this work for mixing in stratified flows and brief conclusions are drawn in § 4.

## 2. Experiments

We show the experimental set-up in figure 1. We use a Taylor–Couette cell whose inner and outer radii are  $R_I = 4$  cm and  $R_O = 9$  cm, respectively. The inner cylinder is stationary whereas the outer cylinder rotates at a constant angular velocity  $\Omega$ .

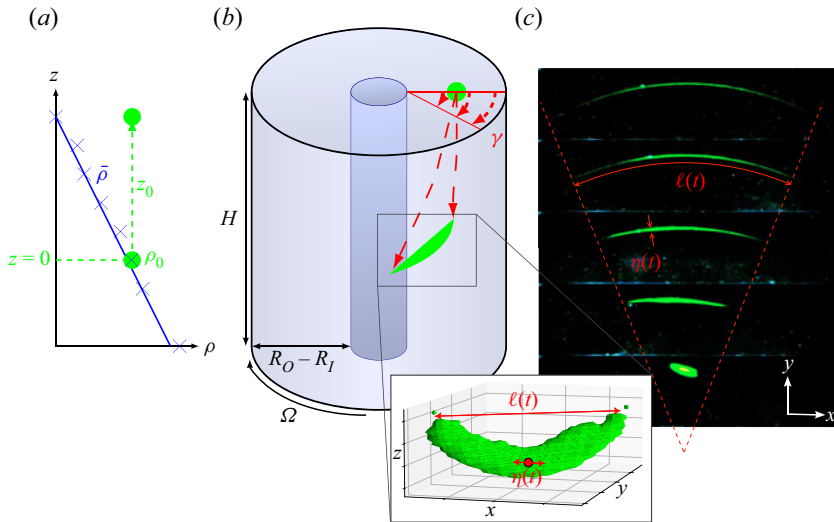


Figure 1. (a) Typical ambient density profile: crosses correspond to experimental measurements; the solid line corresponds to a linear fit. (a,b) Experimental set-up: a (green) blob of density  $\rho_0$  is released at the surface of the cell, experiencing a local azimuthal velocity radial shear rate  $\gamma$ . The distance  $z_0$  is the distance from the surface to the location where the ambient density is  $\rho_0$ . The inset of (b) shows a reconstruction corresponding to an iso-concentration surface, defining the lamella's time-dependent length  $\ell$  and width  $\eta \ll \ell$ . This reconstruction consists of multiple frames as the lamella rotates through the laser sheet. (c) Top (offset) views of the settling lamella at five different times (separated by a rotation period; an artificial shift in the  $y$ -direction has been added between each frame), showing  $\ell(t)$  to increase approximately linearly (red dashed lines).

By construction, the flow is also stable with respect to centrifugal instability (Chandrasekhar 1961) and is therefore laminar. This configuration gives rise to an azimuthal velocity profile in the radial direction,  $V_\theta(r) = Ar + B/r$  (with  $A = \Omega R_O / (R_O^2 - R_I^2)$  and  $B = -\Omega R_O R_I^2 / (R_O^2 - R_I^2)$ ). As the settling lamella has initial (and hence maximum) width  $s_0 \simeq 2.5 \times 10^{-3} \text{ m} \ll R_O - R_I$ , it experiences a flow with constant (radial) shear rate  $\gamma := r \partial_r [V_\theta / r] |_{r=R_b} = -2B/R_b^2$  (where  $R_b$  is the radial position at which the blob is deposited), independent of the vertical coordinate  $z$ . We fill the cell with two-thirds glycerol and one-third linearly stratified salt water (as shown in figure 1a) using the double-bucket method, creating a stratification characterised with a buoyancy frequency of  $N^2 \simeq 1.4 \text{ s}^{-2}$ .

The stratification suppresses any significant Ekman pumping during an individual experiment, while the kinematic viscosity of the experimental fluid,  $\nu = 2.6 \times 10^{-5} \text{ m}^2 \text{ s}^{-1}$ , ensures that the Reynolds number  $Re \lesssim 10^{-1}$ , preventing all potential flow instabilities (without glycerol the initial blob quickly transforms into a vortex ring that destabilises through Rayleigh–Taylor-type instabilities and then disintegrates; these are the kinds of instabilities that we aim to damp using a more viscous fluid). The viscosity of the water–glycerol mixture is estimated using parametrisations developed by Cheng (2008) and Volk & Kähler (2018). The molecular diffusivity  $D$  of salt in this mixture is estimated using the Stokes–Einstein formula and found to be  $D \simeq 3.7 \times 10^{-11} \text{ m}^2 \text{ s}^{-1}$ , so that  $Pr \simeq 7.0 \times 10^5$ .

We prepare a blob (using the same mixture) to have density  $\rho_0 (= 1.217 \text{ g cm}^{-3})$ , corresponding to the background density  $\bar{\rho}$  at the height defined as  $z = 0$ , located approximately  $0.5H$  above the bottom of the container to prevent interactions with the bottom boundary. We form the initial blob at the tip of a syringe that is gently brought

towards the surface of the cell. As soon as the blob touches the surface, it is injected into the liquid bulk by the release of surface tension stresses and slowly falls down due to buoyancy forces, as the surface is a distance  $z = z_0$  above the location where  $\bar{\rho} = \rho_0$ . We dye the blob using fluorescein. The molecular diffusivity of the fluorescein in the salt-water-glycerol mixture is estimated to be of order  $D_{fluor} \simeq 1.6 \times 10^{-10} \text{ m}^2 \text{ s}^{-1}$ , so  $(D/D_{fluor})^{1/3} \simeq 0.6$ , implying that the evolution of fluorescein concentration is a good proxy for tracking the evolution of salt concentration and hence density in the settling lamella.

We visualise the settling lamella through laser-induced fluorescence of fluorescein using a fixed vertical blue laser sheet (in the  $x$ - $z$  plane, perpendicular to the flow) that the lamella crosses as it falls. The data are acquired using a low-light-sensitive camera appropriately calibrated (see Meunier 2020). The set-up has a spatial resolution of  $2.0 \times 10^{-5} \text{ m pixels}^{-1}$ , which ensures that the key Batchelor scale  $\eta_B \simeq s_0 Pe^{-1/3}$  (see e.g. Souzy *et al.* 2018) is resolved for the range of parameters studied here,  $\eta_B \in [5 \times 10^{-5} \text{ m}, 9 \times 10^{-5} \text{ m}]$ .

Figure 1(c) presents (offset) top-view visualisations of the blob when it is stretched by the shear, showing that the length  $\ell(t)$  of the blob increases approximately linearly at late times, as determined through the kinematics (for a constant shear rate  $\gamma$ ) by

$$\ell = s_0 \sqrt{1 + (\gamma t)^2}. \quad (2.1)$$

Figure 2 shows qualitatively the vertical trajectory of a blob as it settles for various shear rates  $\gamma$ , associated with different rotation rates  $\Omega$ . In the absence of shear, the blob falls down until its position  $z_b$  actually reaches  $z = 0$ , where its (initial, unmixed) density  $\rho_0$  is equal to the background density  $\bar{\rho}(z = 0)$  (figure 2a). The main blob is followed by a thin filament reorganising into small secondary blobs, which will not be considered in this paper. This might be the consequence of a Rayleigh-Plateau-type instability, the fluorescein potentially changing the surface tension of the fluid in the settling blob. The (unsheared) blob also seems to start forming a dense-core vortex ring, as can be seen for instance in the middle section of figure 2(a). Such a structure is known to enhance mixing with the surrounding fluid, as discussed in Linden (1973), Camassa *et al.* (2013) and Olsthoorn & Dalziel (2017) in the case of strongly stratified interfaces, but this effect was not seen here, at least within the precision of our measurements, viscosity potentially preventing the full development of the vortex ring. In the presence of shear ( $\Omega \neq 0$ ), the width  $\eta$  of the blob decreases at early times since the blob is stretched in the along-lamella direction. The drag is therefore higher and diffusion acts sooner, thus reducing the (driving) buoyancy force. As a consequence, the blob falls more slowly, mixes with the surrounding (less dense) fluid and hence stops before reaching  $z = 0$ . This effect is clearly visible in figure 3(a), showing the temporal evolution of the vertical position of the blob. Quantitatively, the final position of the lamella, denoted by  $z_f$ , increases from  $0.1z_0$  to  $0.7z_0$  when the shear increases from 0.1 to  $1 \text{ s}^{-1}$ .

### 3. Model for a mixing lamella

We develop a simple model coupling the vertical motion of a settling lamella with its mixing dynamics and then discuss its implications for mixing more generally. We formulate a time-dependent force balance where  $F_D(t)$  is the drag force,  $F_B(t)$  the buoyancy force,  $\rho_b(t)$  the density of the lamella,  $V_b(t)$  its volume and  $z_b(t)$  its vertical

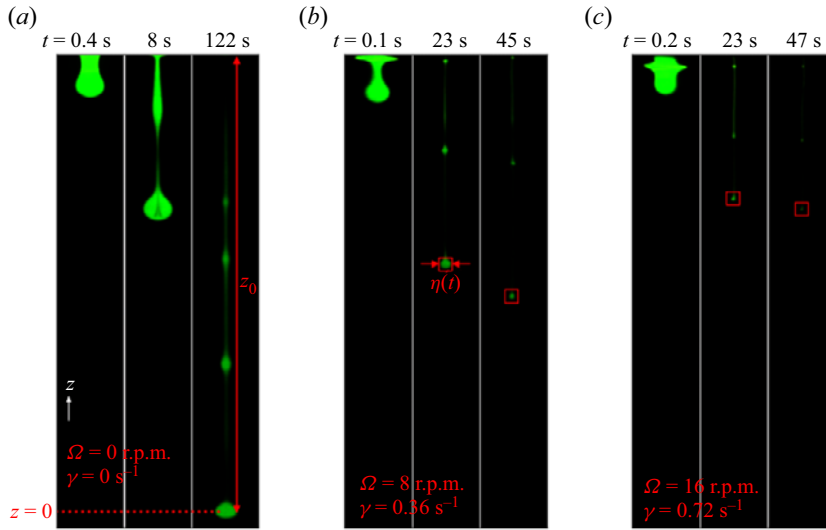


Figure 2. (a–c) Settling of a dyed lamella of initial density  $\rho_0$  released at the surface for different rotation speeds  $\Omega$  of the outer cylinder. The height  $z_0$  corresponds to the vertical distance between the surface and the position  $z = 0$  where the ambient density  $\bar{\rho} = \rho_0$ . Note that in the sheared cases, the blob initially split into a main and a secondary blob. The discussion that follows and the model developed in this work for the settling dynamics of the blob focus on the main blob (framed in red), which does not lose mass except through a weak trailing filament, and we will hence use its total mass as the conserved mass in our model (see § 3).

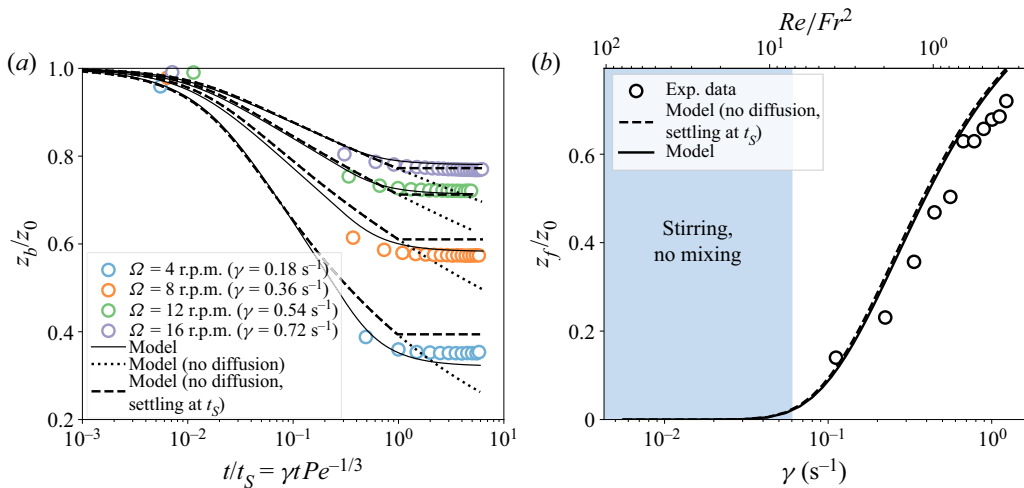


Figure 3. (a) Experimental and theoretical (from (3.4)) vertical trajectories of the settling lamellae for various rotation speeds  $\Omega$ . The position of the blob is scaled by  $z_0$  and time is scaled by the mixing time  $t_S = \gamma^{-1} Pe^{1/3}$  (in dimensional form). The thick black line corresponds to a numerical integration of (3.4). The dotted black line corresponds to the non-diffusive model (3.7). The dashed black line corresponds to the non-diffusive model (3.7) settled at  $t = t_S$ . Note that the data are collected when the maximal concentration point of the lamella crosses the laser sheet, i.e. once per rotation period of the lamella around the set-up, and not continuously. (b) Dimensionless final position of the settling lamella for various shear rates  $\gamma$ . The data are also presented as a function of  $Re/Fr^2$ , a parameter that controls the mixing criterion developed in § 3.3. The dashed black line corresponds to the approximation given by (3.10), whereas the thick black line corresponds to a numerical integration of (3.4). The shaded region corresponds to the range of shear rates  $\gamma$  for which the lamella settles at  $z_f \approx 0$ , i.e. its final density is approximately unchanged.

position:

$$\rho_b V_b \frac{d^2 z_b}{dt^2} = F_D + F_B, \quad (3.1)$$

where

$$F_B = -[\rho_b - \bar{\rho}(z_b)] V_b(t) g, \quad \bar{\rho}(z) = \rho_0 \left(1 - \frac{N^2}{g} z\right) \quad (3.2a,b)$$

and  $N$  is the (constant) buoyancy frequency. The settling velocity  $dz_b/dt$  ensures that the Reynolds number of the wake  $|dz_b/dt|\eta/\nu \lesssim O(10^{-3})$ . In this Stokes regime, the drag force is proportional to the settling velocity and the length of the lamella  $\ell(t)$ :

$$F_D = -\frac{\pi}{6} \alpha \nu \rho_0 \ell(t) \frac{dz_b}{dt} \quad (3.3)$$

using the Boussinesq approximation, fixing the density at the reference value  $\rho_0$ . The drag coefficient  $\alpha$  depends on different parameters of the problem such as the viscosity of the fluid, the settling speed of the lamella and its geometry. It has been taken to be approximately 7, a value that gives good agreement between the experimental data and the theoretical predictions (see [figure 3a](#)). This value of  $\alpha$  can be compared with its theoretical value computed assuming that the lamella is an infinite cylinder of radius  $s_0$  settling at a constant speed  $U$  (see e.g. [Lamb 1932](#)),  $\alpha_{th} = 24/[(1/2) - \gamma_E - \log(Us_0/4\nu)] \simeq 5$  where  $U = O(10^{-3}) \text{ m s}^{-1}$  is the mean vertical velocity of the settling lamella and  $\gamma_E$  is Euler's constant. A better drag model (especially for low shear rates  $\gamma \ll 1$ ) would perhaps consist of a finite-volume drag model for spheroids (that importantly evolves as the shape of the lamella changes) such as that developed by [Chwang & Wu \(1975\)](#). For the sake of simplicity, we did not investigate this option further.

Mass conservation ensures that  $\rho_b V_b = \rho_0 V_0$  where  $V_0 = \pi s_0^3/6$  is the initial volume of the (assumed spherical) blob. Note that in the sheared cases, the blob initially (more precisely, before the first passage of the blob through the laser sheet, i.e. within one half-rotation period) split into a main and a secondary blob. The discussion that follows and the model developed here focus on the main blob (highlighted in red in [figure 2](#)), which does not lose mass except through a weak trailing filament and for which mass conservation thus seems to be valid. Note that we can reconstruct the main blob using multiple images as it rotates through the laser sheet and hence estimate its volume. Using this technique for the second and third passages of the lamella at  $\Omega = 8 \text{ r.p.m.}$  (experiment presented in [figure 2b](#)), we find that, within the error bounds of the method, the volume of the lamella is conserved and is approximately  $3 \times 10^{-9} \text{ m}^3$ . Since these measurements are done before the mixing time (estimated to be 169 s in this particular case), this further supports that conservation of mass is valid for the main blob within the approximations done in this work. Hence, we focus here on the main blob and use its total mass as the conserved mass in our model.

We now non-dimensionalise all quantities using the initial size of the blob  $s_0$  and the shear rate  $\gamma$  so that  $\hat{z}_b \equiv z_b/s_0$ ,  $\hat{z}_0 \equiv z_0/s_0$ ,  $\hat{t} \equiv \gamma t$ ,  $\hat{\rho}_b \equiv \rho_b/\rho_0$ ,  $\hat{N} \equiv N/\gamma$ ,  $\hat{V}_b \equiv V_b/V_0$  and  $\hat{\ell} \equiv \ell/s_0$ , and we obtain

$$\frac{d^2 \hat{z}_b}{d\hat{t}^2} = -\frac{\alpha}{Re} \hat{\ell} \frac{d\hat{z}_b}{d\hat{t}} - \left(\frac{1}{Fr^2 \hat{\rho}_b}\right) \hat{z}_b - \beta \left(1 - \frac{1}{\hat{\rho}_b}\right) \quad \text{with } \hat{\ell} = \sqrt{1 + \hat{t}^2}, \quad (3.4)$$

where

$$Re := \frac{\gamma s_0^2}{\nu}, \quad Fr := \frac{\gamma}{N}, \quad \beta := \frac{g}{s_0 \gamma^2}. \quad (3.5a-c)$$

Here  $Fr$  is a Froude number that compares the buoyancy time scale  $1/N$  to the shear time  $\gamma^{-1}$ , while the parameter  $\beta$  compares the inviscid free-fall time  $\sqrt{s_0/g}$  to the shear time. For  $\gamma = 0.1 \text{ s}^{-1}$ , we have  $Re \simeq 10^{-2}$ ,  $Fr^2 \simeq 10^{-1}$ ,  $\beta \simeq 10^4$  and  $Pe \simeq 10^4$ . For  $\gamma = 1 \text{ s}^{-1}$ , we have  $Re \simeq 10^{-1}$ ,  $Fr^2 \simeq 10$ ,  $\beta \simeq 10^2$  and  $Pe \simeq 10^5$ . Thus, this experiment can access weakly stratified (high  $Fr$ ) and strongly stratified (low  $Fr$ ) laminar flow regimes, at large  $Pe$ . Note that another important dimensionless parameter of our system is the Archimedes number (comparing buoyancy and viscous forces), defined as

$$Ar := \frac{gs_0^3 [\rho_0 - \bar{\rho}(z_0)] / \bar{\rho}(z_0)}{\nu^2}, \quad (3.6)$$

where  $\bar{\rho}(z_0)$  is the density of the surrounding fluid at the injection point. The Archimedes number was estimated to be approximately 4. In the rest of the paper, we will work with dimensionless quantities (unless otherwise stated) and will therefore drop the hats for clarity.

### 3.1. Non-diffusive dynamics

Given the low values of  $Re \ll 1$ , the settling dynamics is over-damped, so inertia can be neglected in (3.4) (i.e.  $d^2z_b/dt^2 \simeq 0$ ). Considering the initial regime when the deforming lamella has not yet mixed and its density is still unaltered (i.e. dimensionless  $\rho_b = 1$ ),

$$z_b(t) = z_0 \left[ \sqrt{1 + t^2} + t \right]^{-Re/(\alpha Fr^2)}. \quad (3.7)$$

We plot this prediction in figure 3(a) (dotted lines). Unlike in the experiment, (3.7) predicts that  $z_b \rightarrow 0$  as  $t \rightarrow \infty$ . Indeed, in the absence of diffusion the blob is always denser than the surrounding fluid for  $z_b > 0$ . We thus need to introduce diffusive effects to predict the final position correctly.

### 3.2. Diffusive dynamics

Figure 4(a) shows the temporal evolution of the maximal dye concentration  $C_{max}$  and the corresponding blob width. The shear stretches the blob into a thin lamella, enhancing diffusion and leading to a decrease of the maximal concentration. We know that for the linear stretching stirring protocol studied here, the diffusion problem (and hence the maximal concentration) depends on the Ranz time  $\tau$  (Ranz 1979; Villermaux 2019):

$$C_{max} = C_0 \operatorname{erf} \left[ \frac{1}{4\sqrt{\tau}} \right], \quad \text{where } \tau = \frac{1}{Pe} \int \ell(t)^2 dt = \frac{1}{Pe} \left[ t + \frac{t^3}{3} \right] \quad (3.8)$$

and  $C_0$  is the initial concentration of dye in the blob. We plot this prediction with solid lines in figure 4(a). There is excellent agreement with the experimental measurements even though the prediction ignores dynamic buoyancy effects.

The diffusive width of the lamella is equal to the Batchelor thickness given by (see Souzy *et al.* 2018; Villermaux 2019)

$$\eta = \frac{1}{\ell} \sqrt{1 + 4\tau} = \sqrt{\frac{1 + 4(t + t^3/3)/Pe}{1 + t^2}}. \quad (3.9)$$

As shown in figure 4(b),  $\eta$  decreases initially and then increases as  $\sqrt{t}$  when diffusion becomes efficient. Hence, mixing starts when  $\tau > 1$ , i.e. when (in dimensionless form)

## Settling versus mixing in stratified shear flows

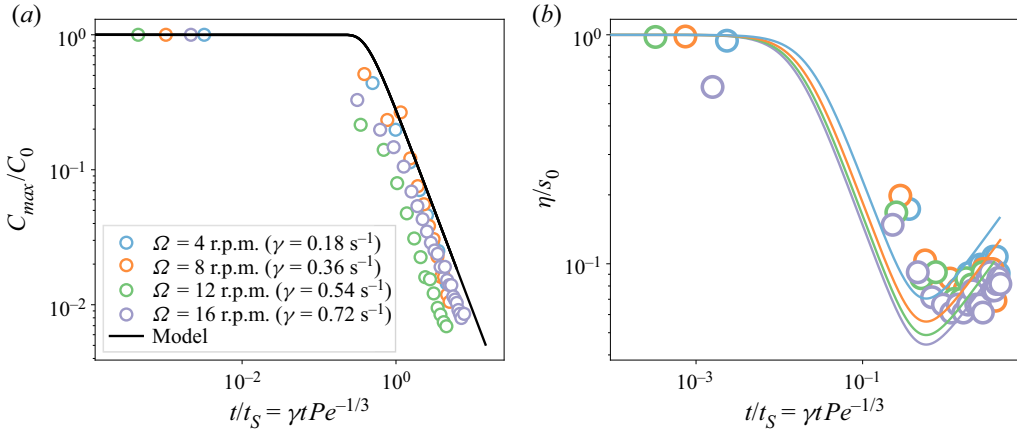


Figure 4. (a) Time evolution of the scaled concentration of dye and (b) scaled width of the settling lamella. Time is scaled using the mixing time  $t_S = \gamma^{-1}Pe^{1/3}$  (in dimensional form). The solid lines correspond to the theoretical predictions (3.8) and (3.9). The size of the symbol in (b) is larger than in (a) to take into account the fact that measurements of the lamella's width are more prone to errors, especially as we approach the Batchelor width. Note that the data are collected when the maximal concentration point of the lamella crosses the laser sheet, i.e. once per rotation period of the lamella around the set-up, and not continuously.

$t > t_S$  where  $t_S = Pe^{1/3}$ . Interestingly, the equilibrium position is reached at approximately the same mixing time  $t = t_S$  as shown in figure 3(a). This is because the difference between the lamella's density and the surrounding fluid's density suddenly decreases at  $t = t_S$ , thus cancelling out the buoyancy force and stopping the descent of the blob. As a first approximation, we can assume that the final position  $z_f$  of the settling lamella (formally equal to  $z_b(t \rightarrow \infty)$  where diffusion has been taken into account) is approximated by its predicted position in the absence of diffusion, (3.7), at  $t = t_S$ :

$$z_f \simeq z_b(t_S) = z_0 \left[ \sqrt{1 + Pe^{2/3}} + Pe^{1/3} \right]^{-Re/(\alpha Fr^2)}. \quad (3.10)$$

We compare this theoretical prediction with experimental data in figure 3(b). The prediction slightly overestimates the equilibrium position. Indeed, the lamella does not abruptly stop at the mixing time. However, there is reasonable agreement in both magnitude and trend.

To improve this prediction, we now assume that the (dimensional) density of the lamella  $\rho_b(t)$  decreases towards the density of the surrounding fluid  $\bar{\rho}$  with the same temporal dependence as the maximal concentration, i.e. that for  $t < t_S$  the density of the lamella remains relatively constant but converges towards the density of the surrounding fluid for  $t > t_S$ . In other words, we assume, using dimensional quantities, that

$$\rho_b(t) - \bar{\rho}(z_b) = [\rho_b(0) - \bar{\rho}(z_b)] \operatorname{erf} \left[ \frac{1}{4\sqrt{\tau}} \right]. \quad (3.11)$$

Rewriting  $\bar{\rho}$  from (3.2a,b) in dimensionless form yields

$$\rho_b(t) = 1 - \frac{1}{\beta Fr^2} z_b + \frac{1}{\beta Fr^2} z_b \operatorname{erf} \left[ \frac{1}{4\sqrt{\tau}} \right]. \quad (3.12)$$

Using this expression for the lamella's time-dependent density, the trajectory of the lamella can no longer be derived theoretically from (3.4). We solve the system numerically using a

backward differentiation method with adaptive time-stepping and plot solutions for various values of the shear rate  $\gamma$  in [figure 3\(a\)](#) (solid lines), demonstrating excellent agreement with the overall time evolution of the vertical trajectory of the blob.

### 3.3. Implications for mixing

The final density of the lamella, and hence the relative amount of mixing it has experienced, can be inferred from the lamella's equilibrium position. The closer the equilibrium position is to its initial position  $z_0$ , the more the lamella has mixed with the surrounding fluid. In that sense,  $z_f/z_0$  in its dimensionless form may be interpreted as a 'mixing efficiency', particularly as it is exactly equal to the ratio between the increase of the background potential energy and the available potential energy of the initial blob, even though the only dynamic effect of the buoyancy has been on the (inertialess) settling of the lamella.

For the linear stretching considered here using [\(3.10\)](#), efficient mixing ( $z_f \simeq z_0$ ) requires

$$\frac{Re \ln(Pe)}{Fr^2} \ll 3\alpha = O(10). \tag{3.13}$$

This mixing criterion incorporates all the effects involved in the problem. A strong stratification (large  $N$ ) must be compensated for by a large shear  $\gamma$  to meet a given efficiency (i.e. keeping  $Fr$  fixed). Viscous damping (large  $\nu$ ) will actually slow down settling and favour efficiency. Significantly, weak diffusion (small  $D$  and hence larger  $Pe$ ) will delay mixing, thus reducing efficiency (consistent with simulations as discussed in the Introduction), although through a weak, but nevertheless quantifiable, logarithmic correction, as is classically the case for all stretching-enhanced diffusion processes (Villermaux [2019](#)).

### 3.4. Generalisation

The above results are valid for a linear shear (i.e.  $\ell(t) \sim t$  at large times), but are readily generalised to any stretching flow. For a given  $\ell(t)$ , from [\(3.4\)](#), for times  $t \leq t_S$  we can obtain the general expression (in the absence of diffusion and in the  $Re \ll 1$  regime)

$$z_b(t) = z_0 \exp \left[ -\frac{Re}{\alpha Fr^2} \int_0^t \frac{dt'}{\ell(t')} \right]. \tag{3.14}$$

For example, if the lamella is exponentially stretched so that  $\ell(t) = e^t$ , the position  $z_b(t_S)$  is

$$z_f \simeq z_b(t_S) = z_0 \exp \left[ -\frac{Re}{\alpha Fr^2} \left( 1 - \frac{1}{\sqrt{Pe}} \right) \right] \tag{3.15}$$

since the mixing time  $t_S = \ln(Pe)/2$  (Batchelor [1959](#); Villermaux [2019](#)) in that case. Although consistent with the linear stretching case ( $z_f$ , and hence the efficiency, monotonically decreases as  $Pr$  increases), the final position converges to a finite value  $z_0 \exp[-Re/(\alpha Fr^2)]$  in the limit  $Pe \rightarrow \infty$ . Perhaps surprisingly, the blob does not reach  $z = 0$  as  $D \rightarrow 0$  since the drag increases so rapidly. Very interestingly, [\(3.15\)](#) demonstrates that when the elongation is sufficiently rapid (exponential), the final equilibrium position  $z_f$  is independent of the Péclet number  $Pe$  as  $Pe \rightarrow \infty$ , since the analogue of the criterion

(3.13), remaining valid as  $D \rightarrow 0$ , is

$$\frac{Re}{Fr^2} \ll \alpha = O(10). \quad (3.16)$$

This result, arising from a deterministic, smooth, non-singular stirring process, has a significant implication for scalar dissipation cascades. A classical ‘law’ of passive scalar turbulence is that  $D|\nabla C|^2$ , where  $C$  is the concentration of the scalar, remains finite as  $D \rightarrow 0$ . Although some counter-examples to this law have been presented (see for example Balmforth & Young 2003), a consistent argument for when this law applies in passive scalar mixing can be formulated (Villermaux 2012, 2019). Essentially, the (finite) mixing time  $t_S$  is independent of  $D$  only when  $\ell(t)$  diverges in a finite time  $t_\star = t_S$ . In the stratified situation considered here, this condition on  $\ell(t)$  is relaxed. As there is an inherent coupling between the lamella settling speed and its density, there is a slowing cascade towards immobility. During this cascade (which does not terminate in finite time) diffusion can disappear, even though diffusion is the actual mechanism driving the density equalisation. There is a highly suggestive analogy with the way that viscosity disappears in the infinitely accelerating cascade towards viscous dissipation in the kinetic energy cascade (Donzis, Sreenivasan & Yeung 2005), leading to the ‘zeroth law of turbulence’.

#### 4. Discussion

We have explored the fundamental small-scale mechanisms of diffusive mixing in stratified shear flows by analysing the settling of a dense blob in a simple experimental flow geometry that is constructed to decouple the blob stretching dynamics (driven by horizontal velocity gradients) and the settling (driven by vertical buoyancy forces). We have shown that such mixing results from the simultaneous and competing effects of stretching-enhanced diffusion, which tends to mix fluid parcels with different densities, and restoring buoyancy forces, which tend to return vertically perturbed parcels to their initial position and hence limit mixing. Note that the regime studied here is not Taylor–Aris dispersion (Taylor 1953; Aris 1956), since the blob width never reaches the gap width. This is a pre-Taylor–Aris dispersion regime characterised by a stretching-enhanced diffusion process.

We have shown that the blob settling dynamics is amenable to a standard mixing analysis in a shear flow that naturally leads to a criterion for mixing efficiency, (3.13) and (3.16). This criterion confirms that mixing by overturning density gradients is prevented in sufficiently strongly stratified flows and that mixing in stratified shear flows is principally controlled by velocity-shear-induced stretching. Furthermore, it also explicitly captures the dependence of the mixing efficiency on the molecular diffusivity of the scalar being mixed as well as the previously empirically observed property that mixing efficiency decreases with the Prandtl number  $Pr$ . It confirms (yet again) that ‘history matters’ in mixing problems, as the time-integrated effects of both settling and stretching must be tracked to quantify accurately the associated diffusive irreversible mixing, and that the exceptionally small-scale diffusive processes are crucially important for mixing (Villermaux 2019; Caulfield 2021).

The configuration studied here involves a laminar, time-independent flow, for which the viscosity was large enough to neglect the buoyancy-driven coupling between the density and velocity fields, the vertical settling velocity being sufficiently small. A natural question is therefore whether the mixing criterion derived here remains relevant for unsteady flows at larger Reynolds numbers, as commonly arise in geophysics (Gregg *et al.* 2018; Caulfield 2021). Concentrating on the dynamics of a lamella enables, at least in some sense, the

abstraction of the Reynolds number by incorporating the complexity of the flow in the laws describing its stretching. However, as inertial effects become important and the flow becomes turbulent, the one-way coupling considered here will inevitably become two-way, with the evolution of the density of lamellae dynamically influencing the velocity field, a key difference between stratified and unstratified flows. However, following Batchelor (1959), we speculate that our analysis remains valid at sufficiently small scales, and specifically in the interval of scales between the Kolmogorov scale  $\eta_K = (\nu^3/\epsilon)^{1/4}$  ( $\epsilon$  being the dissipation rate of turbulent kinetic energy), where (loosely) velocity gradients are smoothed by viscosity, and the Batchelor scale  $\eta_B = \eta_K/Pr^{1/2}$ , where scalar gradients are diffused, suggesting that exceptionally small-scale diffusive processes are crucially important for mixing even in strongly turbulent flows. Such an interval occurs in the oceans where  $Pr = O(10)$ , for example. Finally, if an isolated lamella is the ‘quantum’ of mixing, randomly stirred mixtures typically involve the aggregation of multiple nearby lamellae (Villermaux & Duplat 2003), thus forming larger, apparently uniform-in-concentration regions in the flow (Villermaux & Duplat 2006). The dynamics of such regions in stratified shear flows is a fascinating topic left for future work.

**Acknowledgements.** N.P. would like to thank the people at IRPHE, where this project was initiated, for hosting him for three months. Thanks are also due to four anonymous reviewers, whose comments have greatly improved the manuscript.

**Funding.** This project has received funding from the European Union’s Horizon 2020 research and innovation programme under the Marie Skłodowska-Curie grant agreement no. 956457.

**Declaration of interests.** The authors report no conflict of interest.

#### Author ORCIDs.

- ① Nicolaos Petropoulos <https://orcid.org/0000-0002-8585-7139>;
- ① Colm-cille P. Caulfield <https://orcid.org/0000-0002-3170-9480>;
- ① Patrice Meunier <https://orcid.org/0000-0002-5034-6056>;
- ① Emmanuel Villermaux <https://orcid.org/0000-0001-5130-4862>.

#### REFERENCES

- ARIS, R. 1956 On the dispersion of a solute in a fluid flowing through a tube. *Proc. R. Soc. Lond. A* **235** (1200), 67–77.
- BALMFORTH, N.J. & YOUNG, W.R. 2003 Diffusion-limited scalar cascades. *J. Fluid Mech.* **482**, 91–100.
- BATCHELOR, G.K. 1959 Small-scale variation of convected quantities like temperature in turbulent fluid. Part 1. General discussion and the case of small conductivity. *J. Fluid Mech.* **5** (1), 113–133.
- CAMASSA, R., KHATRI, S., MCLAUGHLIN, R., MERTENS, K., NENON, D., SMITH, C. & VIOTTI, C. 2013 Numerical simulations and experimental measurements of dense-core vortex rings in a sharply stratified environment. *Comput. Sci. Disc.* **6** (1), 014001.
- CAULFIELD, C.P. 2021 Layering, instabilities, and mixing in turbulent stratified flows. *Annu. Rev. Fluid Mech.* **53** (1), 113–145.
- CHANDRASEKHAR, S. 1961 *Hydrodynamic and Hydromagnetic Stability*. Dover.
- CHENG, N.-S. 2008 Formula for the viscosity of a glycerol–water mixture. *Ind. Engng Chem. Res.* **47** (9), 3285–3288.
- CHWANG, A.T. & WU, T.Y.-T. 1975 Hydromechanics of low-Reynolds-number flow. Part 2. Singularity method for Stokes flows. *J. Fluid Mech.* **67** (4), 787–815.
- DONZIS, D.A., SREENIVASAN, K.R. & YEUNG, P.K. 2005 Scalar dissipation rate and dissipative anomaly in isotropic turbulence. *J. Fluid Mech.* **532**, 199–216.
- GREGG, M.C., D’ASARO, E.A., RILEY, J.J. & KUNZE, E. 2018 Mixing efficiency in the ocean. *Annu. Rev. Mar. Sci.* **10**, 443–473.
- LAMB, H. 1932 *Hydrodynamics*, 6th edn. Cambridge University Press.
- LINDEN, P.F. 1973 The interaction of a vortex ring with a sharp density interface: a model for turbulent entrainment. *J. Fluid Mech.* **60** (3), 467–480.

## Settling versus mixing in stratified shear flows

- MEUNIER, P. 2020 Geoinspired soft mixers. *J. Fluid Mech.* **903**, A15.
- MEUNIER, P. & VILLERMAUX, E. 2003 How vortices mix. *J. Fluid Mech.* **476**, 213–222.
- MUNK, W.H. 1966 Abyssal recipes. *Deep-Sea Res.* **13**, 707–730.
- OLSTHOORN, J. & DALZIEL, S.B. 2017 Three-dimensional visualization of the interaction of a vortex ring with a stratified interface. *J. Fluid Mech.* **820**, 549–579.
- RANZ, W.E. 1979 Applications of a stretch model to mixing, diffusion, and reaction in laminar and turbulent flows. *AIChE J.* **25** (1), 41–47.
- RILEY, J.J., COUCHMAN, M.M.P. & DE BRUYN KOPS, S.M. 2023 The effect of Prandtl number on decaying stratified turbulence. *J. Turbul.* **24** (6–7), 330–348.
- SALEHIPOUR, H., PELTIER, W.R. & MASHAYEK, A. 2015 Turbulent diapycnal mixing in stratified shear flows: the influence of Prandtl number on mixing efficiency and transition at high Reynolds number. *J. Fluid Mech.* **773**, 178–223.
- SMYTH, W.D., MOUM, J.N. & CALDWELL, D.R. 2001 The efficiency of mixing in turbulent patches: inferences from direct simulations and microstructure observations. *J. Phys. Oceanogr.* **31**, 1969–1992.
- SOUZY, M., ZAÏER, I., LHUISSIER, H., LE BORGNE, T. & METZGER, B. 2018 Mixing lamellae in a shear flow. *J. Fluid Mech.* **838**, R3.
- TAILLEUX, R. 2013 Available potential energy and exergy in stratified fluids. *Annu. Rev. Fluid Mech.* **45**, 35–58.
- TAYLOR, G.I. 1953 Dispersion of soluble matter in solvent flowing slowly through a tube. *Proc. R. Soc. Lond. A* **219** (1137), 186–203.
- VILLERMAUX, E. 2012 On dissipation in stirred mixtures. *Adv. Appl. Mech.* **45**, 91–107.
- VILLERMAUX, E. 2019 Mixing versus stirring. *Annu. Rev. Fluid Mech.* **51** (1), 245–273.
- VILLERMAUX, E. & DUPLAT, J. 2003 Mixing as an aggregation process. *Phys. Rev. Lett.* **91** (18), 184501.
- VILLERMAUX, E. & DUPLAT, J. 2006 Coarse grained scale of turbulent mixtures. *Phys. Rev. Lett.* **97** (14), 144506.
- VOLK, A. & KÄHLER, C.J. 2018 Density model for aqueous glycerol solutions. *Exp. Fluids* **59** (5), 75.
- WINTERS, K.B., LOMBARD, P.N., RILEY, J.J. & D'ASARO, E.A. 1995 Available potential energy and mixing in density-stratified fluids. *J. Fluid Mech.* **289**, 115–128.
- WUNSCH, C. & FERRARI, R. 2004 Vertical mixing, energy, and the general circulation of the oceans. *Annu. Rev. Fluid Mech.* **36**, 281–314.